

Efficiency of eclogite removal from continental lithosphere and its implications for cratonic diamonds

Yantao Luo* and Jun Korenaga*

Department of Earth and Planetary Sciences, Yale University, P.O. Box 208109, New Haven, Connecticut 06520-8109, USA

ABSTRACT

Continental lithospheric mantle (CLM) may have been built from subducted slabs, but the apparent lack of concurrent oceanic crust in CLM, known as the mass imbalance problem, remains unresolved. Here, we present a simple dynamic model to evaluate the likelihood of losing dense eclogitized oceanic crust from CLM by gravitational instability. Our model allowed us to assess the long-term evolution of such crust removal, based on how thermal and viscosity profiles change over time across the continental lithosphere. We found that the oceanic crust incorporated early into CLM can quickly escape to the asthenosphere, whereas that incorporated after a certain age would be preserved in CLM. This study provides a plausible explanation for the mass imbalance problem posed by the oceanic ridge origin hypothesis of CLM and points to the significance of preservation bias inherent to the studies of cratonic diamonds.

INTRODUCTION

Several hypotheses have been proposed for the origin of continental lithospheric mantle (CLM), including plume-type magmatism, convergent boundary magmatism, and ocean ridge-type magmatism, among which the ocean ridge origin is most consistent with petrological and geochemical observations (Kelemen et al., 1998; Simon et al., 2007; Rollinson, 2010; Herzberg and Rudnick, 2012; Pearson and Wittig, 2014; Su and Chen, 2018). In addition, a recent global compilation of major-element data in mantle xenoliths showed a trend of increasingly depleted CLM with age (Servali and Korenaga, 2018), which conforms to the prediction of the ocean ridge origin hypothesis. Hotter mantle in the Archean resulted in a higher degree of melting beneath mid-ocean ridges, producing highly depleted mantle residues (Korenaga, 2006; Herzberg and Rudnick, 2012), some of which may have been incorporated into CLM during subduction.

However, the presence of highly depleted mantle xenoliths beneath cratons is rarely accompanied by observations of their complementary melt products, and this issue is known as the mass imbalance problem of cratonic lithosphere (Herzberg and Rudnick, 2012). In the context of

the oceanic ridge origin, a high degree of melting beneath mid-ocean ridges produces not only highly depleted mantle residue but also thick oceanic crust, which should also be incorporated into CLM and eclogitized under pressure. The presence of eclogite inclusions is observed in cratonic diamonds with ages younger than 3 Ga (Shirey and Richardson, 2011). One explanation is that there was no plate tectonics and thus no CLM with an oceanic ridge origin before 3 Ga, but this explanation may overlook the possibility that the oceanic crust incorporated into CLM at earlier times was simply lost due to gravitational instability. Numerical modeling by Percival and Pysklywec (2007) showed that a narrow horizontal slab of eclogite lying between cratonic crust and depleted peridotite lithosphere could sink rapidly into the asthenosphere in a few tens of million years. However, their exploration of relevant model parameter space was limited, making it difficult to draw general conclusions on the fate of oceanic crust in CLM.

In this study, we addressed the mass imbalance problem in an alternative setting, where parts of oceanic lithosphere are broken off during subduction and then imbricated below the continent to form CLM (Fig. 1A). This scenario follows closely what has been suggested from studies of mantle xenoliths and cratonic diamonds (Pearson and Wittig, 2008; Stachel and Harris, 2008). Without loss of much general-

ity, we simplified this imbrication scenario into a uniform vertical stacking model (Fig. 1B). Negative buoyancy due to a density difference between the eclogitized oceanic crust and the surrounding lithospheric mantle will result in the descent of the oceanic crust, which is regulated by viscous drag from the surrounding mantle. To evaluate the magnitude of viscous drag, we first estimated the temporal evolution of the continental geotherm to constrain the viscosity profile of lithospheric mantle at different ages. Then, we calculated the descent velocity of oceanic crust. From this, we determined the time needed for the oceanic crust to escape from the continental lithosphere as a function of its age of incorporation. Finally, we examined the impact of this crust removal mechanism for cratonic diamonds and their inclusions, as well as its implications for the onset of plate tectonics during Earth history.

METHOD AND RESULTS

Temperature

The viscosity profile of mantle material depends strongly on pressure and temperature. Pressure is straightforward to estimate and remains relatively constant over time. The temperature of oceanic lithosphere imbricated to CLM is expected to equilibrate with the continental geotherm within a diffusion time scale of 100 million years (i.e., the same time scale to grow the oceanic lithosphere by conductive cooling). Thus, the evolution of the continental geotherm governs how the viscosity profile of CLM would change with time. We solved the following one-dimensional (1-D) heat conduction equation (Jaupart and Mareschal, 2015),

$$\lambda(T) \frac{dT}{dz} = Q(z), \quad (1)$$

where $\lambda(T)$ is temperature-dependent thermal conductivity, and $Q(z)$ is depth-dependent heat flow, with temperature boundary conditions at the surface and at 250 km depth. Following the

*E-mails: yantao.luo@yale.edu; jun.korenaga@yale.edu

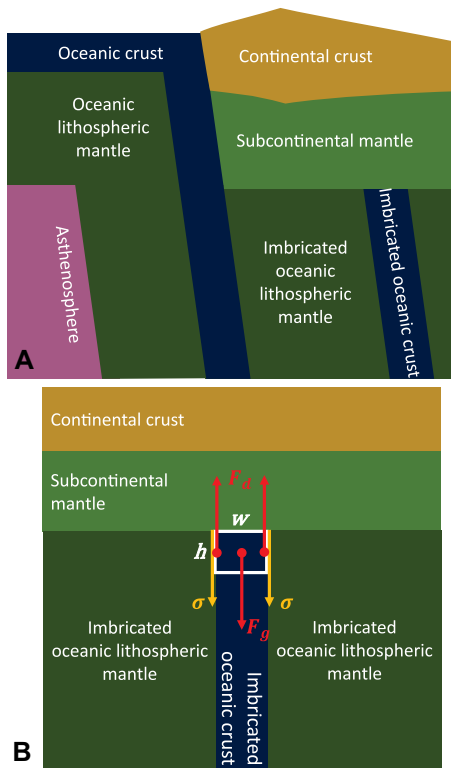


Figure 1. (A) Schematic diagram showing oceanic origin of continental lithospheric mantle (CLM), i.e., the scenario assumed in this study, based on the models of Helms-taedt and Schulze (1989) and Stachel and Harris (2008). Only features that are essential to our model are shown here. (B) Schematic diagram illustrating our simplified model setting with oceanic crust embedded in vertically stacked oceanic lithospheric mantle. F_g is negative buoyancy, and F_d is viscous drag force, where σ is stress acting on surrounding mantle by descending crust with thickness w . White rectangle with height h represents the segment used to estimate the Stokes flow velocity.

approach of Chu and Korenaga (2012), the surface temperature was fixed at 25 °C, and the bottom temperature was set according to mantle potential temperature with an adiabatic gradient of 0.5 °C/km. The potential temperature increases with age and peaks at around 3 Ga, according to geodynamic calculations (Korenaga, 2008) and petrologic observations (Herzberg et al., 2010). Temperature-dependent thermal conductivities for the crust and the mantle were adopted from Whittington et al. (2009) and McKenzie et al. (2005), respectively. The Moho was fixed at 40 km. We used the average present-day heat production of 0.5 mW/m³ for the crust and 0.028 mW/m³ for the lithospheric mantle and adopted a three-layer crust model where the shallowest layer contributed 60% of crustal heat production (Rudnick et al., 1998). We then calculated heat production in the past based on the decay constants of radiogenic isotopes and obtained the temporal evolution of the continental geotherm (Fig. 2A). The result-

ing geotherms are consistent with the geothermometry of cratonic diamonds (Fig. S1 in the Supplemental Material¹). Model parameters for the geotherm calculation, as well as the viscosity calculation described next, are fully described in the Supplemental Material.

Viscosity

The rheology of the upper mantle is dominated by that of olivine because olivine is the weakest and also the most abundant phase in the upper mantle (Karato and Wu, 1993). We calculated viscosity profiles based on both the diffusion creep of olivine aggregates,

$$\eta_{\text{diff}} = A^{-1} d^p \exp\left(\frac{E + PV}{RT}\right), \quad (2)$$

and the dislocation creep,

$$\eta_{\text{dis}} = A^{-1} \sigma^{1-n} \exp\left(\frac{E + PV}{RT}\right), \quad (3)$$

where d is grain size, σ is stress, P is pressure, T is temperature, and R is the gas constant. We adopted the pre-exponential constants A , the grain size exponent p , the stress exponent n , and the activation energy E from model OL-DB₂ of Jain et al. (2019), which corresponds to dry conditions, because the surrounding mantle in this case is highly depleted and thus expected to be dry. For grain size d , a typical mantle xenolith value of 5 mm was used (Ave Lallemand et al., 1980). The activation volume, V , was the most uncertain flow-law parameter, which was not estimated by the global inversion of Jain et al. (2019). Because laboratory-based estimates to date vary from 2.5 cm³/mol to 27 cm³/mol under dry conditions (Hirth and Kohlstedt, 2003; Durham et al., 2009; Dixon and Durham, 2018), the activation volumes of 10, 20, and 30 cm³/mol were tested in this study.

The stress exerted by dense oceanic crust on the surrounding mantle (Fig. 1B) may be expressed as

$$\sigma = \frac{1}{2} \Delta \rho g w, \quad (4)$$

where $\Delta \rho$ is the density difference between oceanic crust and lithospheric mantle, g is gravitational acceleration, and w is the thickness of oceanic crust. The density difference is ~200 kg/m³, based on the bulk density of eclogitic crust (Aoki and Takahashi, 2004). The thickness of oceanic crust depends on the degree of melting beneath mid-ocean ridges and is thus time dependent. Using the mantle melting model described by Korenaga (2006), we calculated the degree of melting and the

¹Supplemental Material. Details of model parameters and supporting figures. Please visit <https://doi.org/10.1130/GEOL.S.13262786> to access the supplemental material, and contact editing@geosociety.org with any questions.

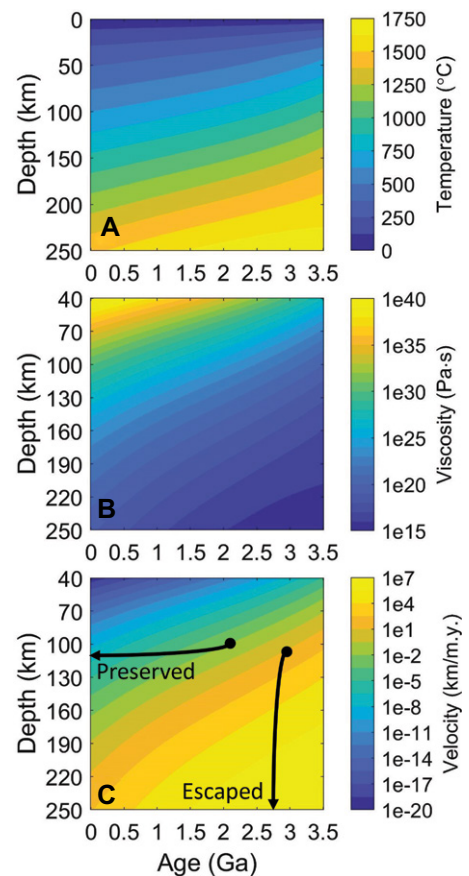


Figure 2. (A) Temporal evolution of continental geotherm. (B) Temporal evolution of viscosity profile calculated based on temperature shown in A, with dislocation creep and activation volume of 20 cm³/mol. (C) Temporal evolution of descent velocity calculated based on viscosity shown in B, with segment height of 20 km. Two contrasting fates of oceanic crust are also shown schematically.

thickness of oceanic crust from mantle potential temperature. For the present-day case, ~7-km-thick oceanic crust produces stress of ~7 MPa, and dislocation creep results in a much lower viscosity than diffusion creep. The oceanic crust in the past would be thicker and produce higher stress, and so dislocation creep remained the dominant deformation mechanism in our model. The temporal evolution of the viscosity profile in the surrounding mantle was thus calculated with dislocation creep (Fig. 2B).

Descent Velocity

Because viscosity changes by several orders of magnitude across the continental lithosphere, different parts of oceanic crust descend at different speeds, with deeper parts sinking faster. Such differential velocity, when combined with the nonlinear rheology of eclogite, would lead to necking instability (e.g., Zuber and Parmentier, 1986; see also Fig. S2). We thus divided the oceanic crust into multiple segments with height

h , and the overall viscous drag force applied on each segment was represented by the drag force at the midpoint, as schematically shown in Figure 1B. The descent of each segment could be modeled using Stokes flow with some modifications. We estimated the viscous drag force using the formula for a long slender body (Happel and Brenner, 1983) as

$$F_d = \frac{4\pi\eta vL}{\ln(L/r) + 0.5}, \quad (5)$$

where v is the terminal velocity, and L is the overall length scale of the subduction zone, for which 2500 km, a representative value for an intermediate-sized subduction zone (Schellart et al., 2007), was used. The cross-sectional radius r was calculated by

$$r = \sqrt{\frac{hw}{\pi}}, \quad (6)$$

Where h is the segment height. By equating the viscous drag with the negative buoyancy,

$$F_g = \Delta\rho ghwL, \quad (7)$$

the terminal velocity of the segment may be expressed as

$$v = \frac{\ln\left(L\sqrt{\frac{\pi}{hw}}\right) + 0.5}{4\pi\eta} \Delta\rho ghw. \quad (8)$$

The temporal evolution of descent velocity at different depths is shown in Figure 2C, with a default segment height of 20 km. The dependence of velocity on h is sublinear, so different choices of h in a reasonable range had limited influence (Fig. S3).

Escape Time

Descent velocity increases with depth, but, owing to the nature of secular cooling, it decreases as time proceeds, which results in two contrasting fates of oceanic crust embedded in CLM, as schematically drawn in Figure 2C. If the oceanic crust were incorporated into CLM at early times, it would start to descend with a high velocity, and it could quickly descend into deeper regions gaining even higher velocity, which is a positive feedback. As a result, an early incorporated oceanic crust could rapidly escape into the asthenosphere. On the other hand, if the oceanic crust were incorporated into CLM relatively late, the initial velocity would be small, preventing it from descending into deeper regions quickly, and as time proceeds, the descent velocity would become even smaller, which is a negative feedback. As a result, a late incorporated oceanic crust would eventually be stuck in the lithosphere and thus preserved.

Figure 3 shows the escape time of oceanic crust as a function of its incorporation age, i.e., when imbricated oceanic lithosphere is equilibrated with the cratonic geotherm. The escape

time of oceanic crust is the time needed for its topmost segment to escape from CLM by descending into the asthenosphere, as shown in Figure S4. Considering that the thickness of the preexisting subcontinental mantle is uncertain, the starting depth of the topmost crustal segment was varied, in addition to the activation volume of dislocation creep and the segment height. The effect of varying these model parameters is shown by different curves in Figure 3; in all cases, a sharp transition can be seen from early positive feedback (short escape time) to late negative feedback (long escape time). Immediately following the sharp transition, these curves intersect with a cutoff line at which the incorporation age of oceanic crust equals the escape time. For example, the reference curve intersects the cutoff line at ca. 2.2 Ga. This means that under the conditions assumed in the reference case, the oceanic crust incorporated into CLM at ca. 2.2 Ga would need ~2.2 b.y. to escape. Therefore, the oceanic crust incorporated before this age has already escaped into the asthenosphere, whereas the oceanic crust incorporated after this age is still preserved in CLM. Such an age is referred to as the transition age hereafter.

DISCUSSION

We have presented a simple geodynamic model for the removal of oceanic crust from CLM. The simplicity allowed us to explore the relevant parameter space and understand the varying nature of this process through Earth history. The temperature near the bottom of CLM is mostly controlled by the secular changes in mantle temperature, which gradually increases before 3 Ga and decreases after 3 Ga at rates around 50–100 K/b.y. (Herzberg et al., 2010).

On the other hand, the temperature at shallower regions is more affected by radiogenic heat production in the continental crust, which decreases monotonically as time proceeds. As shown in Figure 2A, the temporal evolution of the continental geotherm is a gradual process, and the Moho temperature drops by less than 300 K in the span of 3.5 b.y. However, viscosity increases exponentially with decreasing temperature, and the descent velocity of oceanic crust decreases drastically as time proceeds. This strong dependence on temperature results in a sharp contrast between the removal of early incorporated oceanic crust and the preservation of late incorporated oceanic crust.

The fact that the gradual temporal evolution of the geotherm can cause a sudden change in the fate of embedded oceanic crust provides a plausible explanation for the mass imbalance problem involved in the oceanic ridge origin hypothesis of CLM. It also underscores the significance of preservation bias in the geological record (Korenaga, 2018). For the range of parameters explored in this study, the transition age varied from ca. 1.5 Ga to ca. 3 Ga. The transition age can be quite different depending on the set of parameters used, but the sharpness of this transition is likely to persist (Fig. 3). Whenever the transition age is, it could introduce a sudden discontinuity in some observables instead of a gradual evolution. Shirey and Richardson (2011), for example, suggested that the Wilson cycle did not start until 3 Ga because eclogitic diamond older than 3 Ga is not observed. However, according to our results, the absence of older eclogitic diamond may instead reflect the complete removal of early diamondiferous eclogitic crust from CLM. Similarly, the absence of mass-independently fractionated sulfur

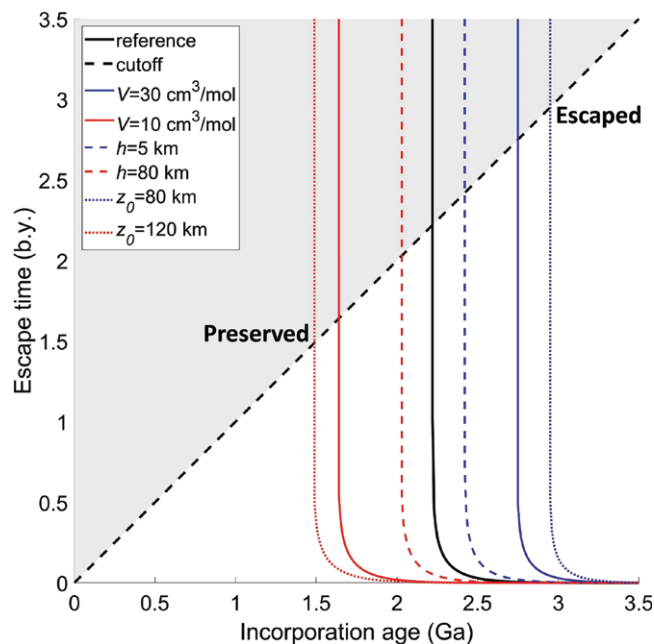


Figure 3. Escape time of oceanic crust as a function of its incorporation age, with the range of parameters tested. Thick solid curve is the reference case, with activation volume V of 20 cm^3/mol for dislocation creep regime, segment height h of 20 km, and starting depth z_0 of 100 km. Red and blue solid curves were calculated by changing the activation volume only. Similarly, dashed curves are for different segment heights, and dotted curves are for different starting depths. Black dashed line is the cutoff line at which the incorporation age of oceanic crust equals escape time.

isotopes in 3.5 Ga diamonds (Smit et al., 2019) does not necessarily mean that ancient CLM was not constructed by subduction-related processes. If sediments on top of oceanic crust, which are an important carrier of the sulfur signal, were also incorporated into CLM, they were likely to be removed by the sinking of dense eclogitized crust, which must have dragged part of the surrounding materials. There are a number of proxies for the operation of plate tectonics in the deep time (e.g., Korenaga, 2013), and the possibility of preservation bias becomes particularly important when evaluating the strength of a given proxy.

The causal relationship between the gradual change of the geotherm and the sudden change of oceanic crust preservation is an enlightening example showing that the continuous evolution of Earth and its physical states can sometimes result in discontinuous observations. Therefore, careful considerations are warranted before extrapolating a discontinuity in observables to a significant watershed moment in the history of Earth.

ACKNOWLEDGMENTS

This study was supported by Yale University (Connecticut, USA) and U.S. National Science Foundation grant EAR-1753916. We thank Noah Planavsky for discussion on cratonic diamonds and sulfur isotopes, and Laurent Montesi, Claude Hertzberg, Scott King, and Norm Sleep for their constructive reviews and suggestions.

REFERENCES CITED

- Aoki, I., and Takahashi, E., 2004, Density of MORB eclogite in the upper mantle: Physics of the Earth and Planetary Interiors, v. 143–144, p. 129–143, <https://doi.org/10.1016/j.pepi.2003.10.007>.
- Ave Lallemand, H.G., Mercier, J.C.C., Carter, N.L., and Ross, J.V., 1980, Rheology of the upper mantle: Inferences from peridotite xenoliths: Tectonophysics, v. 70, p. 85–113, [https://doi.org/10.1016/0040-1951\(80\)90022-0](https://doi.org/10.1016/0040-1951(80)90022-0).
- Chu, X., and Korenaga, J., 2012, Olivine rheology, shear stress, and grain growth in the lithospheric mantle: Geological constraints from the Kaapvaal craton: Earth and Planetary Science Letters, v. 333–334, p. 52–62, <https://doi.org/10.1016/j.epsl.2012.04.019>.
- Dixon, N.A., and Durham, W.B., 2018, Measurement of activation volume for creep of dry olivine at upper-mantle conditions: Journal of Geophysical Research: Solid Earth, v. 123, p. 8459–8473, <https://doi.org/10.1029/2018JB015853>.
- Durham, W.B., Mei, S., Kohlstedt, D.L., Wang, L., and Dixon, N.A., 2009, New measurements of activation volume in olivine under anhydrous conditions: Physics of the Earth and Planetary Interiors, v. 172, p. 67–73, <https://doi.org/10.1016/j.pepi.2008.07.045>.
- Happel, J., and Brenner, H., 1983, Low Reynolds Number Hydrodynamics: Leiden, Netherlands, Martinus Nijhoff, 553 p., <https://doi.org/10.1007/978-94-009-8352-6>.
- Helmstaedt, H., and Schulze, D.J., 1989, Southern African kimberlites and their mantle sample: Implications for Archean tectonics and lithosphere evolution, in Ross, J., et al., eds., Kimberlites and Related Rocks: Geological Society of Australia Special Publication 14, p. 358–368.
- Herzberg, C., and Rudnick, R., 2012, Formation of cratonic lithosphere: An integrated thermal and petrological model: Lithos, v. 149, p. 4–15, <https://doi.org/10.1016/j.lithos.2012.01.010>.
- Herzberg, C., Condie, K., and Korenaga, J., 2010, Thermal history of the Earth and its petrological expression: Earth and Planetary Science Letters, v. 292, p. 79–88, <https://doi.org/10.1016/j.epsl.2010.01.022>.
- Hirth, G., and Kohlstedt, D.L., 2003, Rheology of the upper mantle and the mantle wedge: A view from the experimentalists, in Eiler, J., ed., Inside the Subduction Factory: American Geophysical Union Geophysical Monograph 138, p. 83–105, <https://doi.org/10.1029/138GM06>.
- Jain, C., Korenaga, J., and Karato, S.-i., 2019, Global analysis of experimental data on the rheology of olivine aggregates: Journal of Geophysical Research: Solid Earth, v. 124, p. 310–334, <https://doi.org/10.1029/2018JB016558>.
- Jaupart, C., and Mareschal, J.C., 2015, Heat flow and thermal structure of the lithosphere, in Schubert, G., ed., Treatise on Geophysics (2nd ed.): Oxford, UK, Elsevier, p. 217–253, <https://doi.org/10.1016/B978-0-444-53802-4.00114-7>.
- Karato, S.-i., and Wu, P., 1993, Rheology of the upper mantle: A synthesis: Science, v. 260, p. 771–778, <https://doi.org/10.1126/science.260.5109.771>.
- Kelemen, P.B., Hart, S.R., and Bernstein, S., 1998, Silica enrichment in the continental upper mantle via melt/rock reaction: Earth and Planetary Science Letters, v. 164, p. 387–406, [https://doi.org/10.1016/S0012-821X\(98\)00233-7](https://doi.org/10.1016/S0012-821X(98)00233-7).
- Korenaga, J., 2006, Archean geodynamics and the thermal evolution of Earth, in Benn, K., Mareschal, J.-C., and Condie, K.C., eds., Archean Geodynamics and Environments: American Geophysical Union Geophysical Monograph 164, p. 7–32, <https://doi.org/10.1029/164GM03>.
- Korenaga, J., 2008, Urey ratio and the structure and evolution of Earth's mantle: Reviews of Geophysics, v. 46, RG2007, <https://doi.org/10.1029/2007RG000241>.
- Korenaga, J., 2013, Initiation and evolution of plate tectonics on Earth: Theories and observations: Annual Review of Earth and Planetary Sciences, v. 41, p. 117–151, <https://doi.org/10.1146/annurev-earth-050212-124208>.
- Korenaga, J., 2018, Crustal evolution and mantle dynamics through Earth history: Philosophical Transactions of the Royal Society: Mathematical, Physical, and Engineering Sciences, v. 376, p. 20170408, <https://doi.org/10.1098/rsta.2017.0408>.
- McKenzie, D., Jackson, J., and Priestley, K., 2005, Thermal structure of oceanic and continental lithosphere: Earth and Planetary Science Letters, v. 233, p. 337–349, <https://doi.org/10.1016/j.epsl.2005.02.005>.
- Pearson, D.G., and Wittig, N., 2008, Formation of Archean continental lithosphere and its diamonds: The root of the problem: Journal of the Geological Society, v. 165, p. 895–914, <https://doi.org/10.1144/0016-76492008-003>.
- Pearson, D.G., and Wittig, N., 2014, The formation and evolution of cratonic mantle lithosphere—Evidence from mantle xenoliths, in Holland, H.D., and Turekian, K.K., eds., Treatise on Geochemistry (2nd ed.): Oxford, UK, Elsevier, p. 255–292, <https://doi.org/10.1016/B978-0-08-095975-7.00205-9>.
- Percival, J.A., and Pysklywec, R.N., 2007, Are Archean lithospheric keels inverted?: Earth and Planetary Science Letters, v. 254, p. 393–403, <https://doi.org/10.1016/j.epsl.2006.11.047>.
- Rollinson, H., 2010, Coupled evolution of Archean continental crust and subcontinental lithospheric mantle: Geology, v. 38, p. 1083–1086, <https://doi.org/10.1130/G31159.1>.
- Rudnick, R.L., McDonough, W.F., and O'Connell, R.J., 1998, Thermal structure, thickness and composition of continental lithosphere: Chemical Geology, v. 145, p. 395–411, [https://doi.org/10.1016/S0009-2541\(97\)00151-4](https://doi.org/10.1016/S0009-2541(97)00151-4).
- Schellart, W.P., Freeman, J., Stegman, D.R., Moresi, L., and May, D., 2007, Evolution and diversity of subduction zones controlled by slab width: Nature, v. 446, p. 308–311, <https://doi.org/10.1038/nature05615>.
- Servali, A., and Korenaga, J., 2018, Oceanic origin of continental mantle lithosphere: Geology, v. 46, p. 1047–1050, <https://doi.org/10.1130/G45180.1>.
- Shirey, S.B., and Richardson, S.H., 2011, Start of the Wilson cycle at 3 Ga shown by diamonds from subcontinental mantle: Science, v. 333, p. 434–436, <https://doi.org/10.1126/science.1206275>.
- Simon, N.S.C., Carlson, R.W., Pearson, D.G., and Davies, G.R., 2007, The origin and evolution of the Kaapvaal cratonic lithospheric mantle: Journal of Petrology, v. 48, p. 589–625, <https://doi.org/10.1093/petrology/egl074>.
- Smit, K.V., Shirey, S.B., Hauri, E.H., and Stern, R.A., 2019, Sulfur isotopes in diamonds reveal differences in continent construction: Science, v. 364, p. 383–385, <https://doi.org/10.1126/science.aaw9548>.
- Stachel, T., and Harris, J.W., 2008, The origin of cratonic diamonds—Constraints from mineral inclusions: Ore Geology Reviews, v. 34, p. 5–32, <https://doi.org/10.1016/j.oregeorev.2007.05.002>.
- Su, B., and Chen, Y., 2018, Making cratonic lithospheric mantle: Journal of Geophysical Research: Solid Earth, v. 123, p. 7688–7706, <https://doi.org/10.1029/2018JB016179>.
- Whittington, A.G., Hofmeister, A.M., and Nabelek, P.L., 2009, Temperature-dependent thermal diffusivity of the Earth's crust and implications for magmatism: Nature, v. 458, p. 319–321, <https://doi.org/10.1038/nature07818>.
- Zuber, M.T., and Parmentier, E.M., 1986, Lithospheric necking: A dynamic model for rift morphology: Earth and Planetary Science Letters, v. 77, p. 373–383, [https://doi.org/10.1016/0012-821X\(86\)90147-0](https://doi.org/10.1016/0012-821X(86)90147-0).

Printed in USA